ACS ENVIRONMENTAL Au
AN OPEN ACCESS JOURNAL OF THE AMERICAN CHEMICAL SOCIETY

pubs.acs.org/environau Article

Elucidating the Role of O_2 Uncoupling in the Oxidative Biodegradation of Organic Contaminants by Rieske Non-heme Iron Dioxygenases

Charlotte E. Bopp, Nora M. Bernet, Hans-Peter E. Kohler, and Thomas B. Hofstetter*

Cite This: *ACS Environ. Au* 2022, 2, 428−440 Read Online

ACCESS | Metrics & More | Article Recommendations | Supporting Information

ABSTRACT: Oxygenations of aromatic soil and water contaminants with molecular O_2 catalyzed by Rieske dioxygenases are frequent initial steps of biodegradation in natural and engineered environments. Many of these non-heme ferrous iron enzymes are known to be involved in contaminant metabolism, but the understanding of enzyme−substrate interactions that lead to successful biodegradation is still elusive. Here, we studied the mechanisms of O_2 activation and substrate hydroxylation of two nitroarene dioxygenases to evaluate enzyme- and substrate-specific factors that determine the efficiency of oxygenated product formation. Experiments in enzyme assays of 2-nitrotoluene dioxygenase (2NTDO) and nitrobenzene dioxygenase (NBDO) with methyl-, fluoro-, chloro-, and hydroxy-substituted nitroaromatic substrates reveal that typically 20−100% of the enzyme's activity involves unproductive paths of O_2 activation with generation of reactive oxygen species through so-called O_2 uncoupling. The ^{18}O and ^{13}C kinetic isotope effects of O_2 activation and nitroaromatic substrate hydroxylation, respectively, suggest that O_2 uncoupling occurs after generation of Fe^{III}-(hydro)peroxo species in the catalytic cycle. While 2NTDO hydroxylates *ortho*-substituted nitroaromatic substrates more efficiently, NBDO favors *meta*-substituted, presumably due to distinct active site residues of the two enzymes. Our data implies, however, that the O_2 uncoupling and hydroxylation activity cannot be assessed from simple structure−reactivity relationships. By quantifying O_2 uncoupling by Rieske dioxygenases, our work provides a mechanistic link between contaminant biodegradation, the generation of reactive oxygen species, and possible adaptation strategies of microorganisms to the exposure of new contaminants.

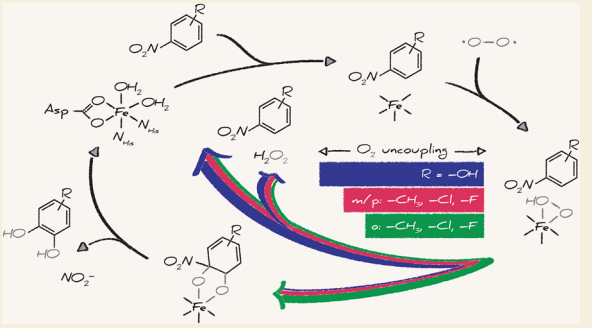

KEYWORDS: *non-heme ferrous iron oxygenases, Rieske oxygenases, biocatalysis, O_2 uncoupling, O_2 activation, kinetic isotope effect, biodegradation*

INTRODUCTION

Oxygenations of aromatic and aliphatic hydrocarbons with molecular O_2 are a frequent initial step of the biodegradation of anthropogenic organic contaminants.[1,2] The oxygenated products are often more polar and more bioavailable than the substrate and can be transformed further in standard metabolic pathways that support microbial growth and energy metabolism.[3,4] Enzymatic oxygenations of recalcitrant aromatic contaminants from a wide range of applications and origins, including pharmaceuticals, industrial chemicals, and explosives,[5−14] are all catalyzed by Rieske dioxygenases (RDOs), a subgroup of non-heme ferrous iron oxygenases involved in many catabolic and biosynthetic processes.[15−29] Even though many contaminant-degrading RDOs are well-known, the factors that determine which enzyme-contaminant combinations lead to successful substrate oxygenation and at which rate contaminant transformation occurs are largely unknown. A generalized assessment of this important reaction path for contaminant biodegradation is therefore hardly possible.

In fact, the role of substrates in the catalytic cycles and kinetic mechanisms of RDOs is still elusive except those used in the characterization of the two prototypical enzymes naphthalene and benzoate dioxyxgenase.[30−32] In contrast to other non-heme ferrous iron oxygenases, RDOs retrieve only two of the four electrons required for the reduction of O_2 from the substrate.[18,22,23] Two additional reduction equivalents originate from NADH oxidation and are supplied through electron transfer proteins via the Rieske cluster.[11,33,34] Hydroxylation of the substrate and, thus, contaminant transformation are preceded by a series of steps responsible for enzymatic O_2 activation (Scheme 1) for which the role of the substrate is

Received: April 15, 2022
Revised: June 1, 2022
Accepted: June 6, 2022
Published: July 7, 2022

https://doi.org/10.1021/acsenvironau.2c00023
ACS Environ. Au 2022, 2, 428−440

Scheme 1. Catalytic Cycle of Nitrobenzene Dioxygenase Shown As Model for Non-Heme Ferrous Iron Rieske Dioxygenases[a]

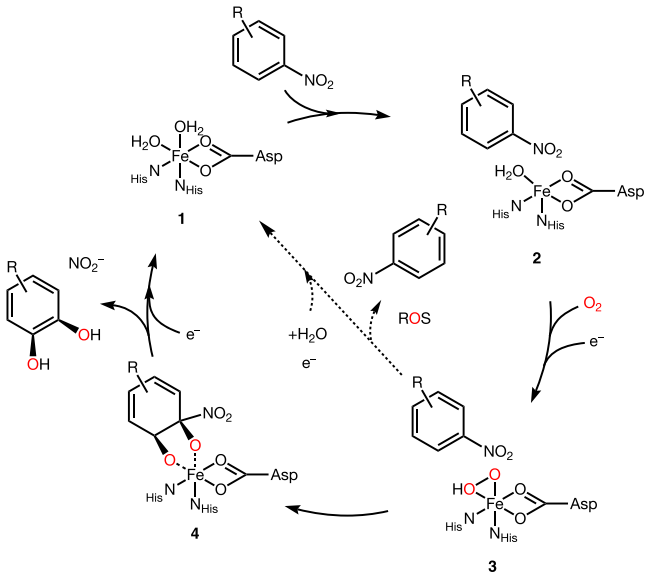

[a]In its resting state (**1**), the non-heme Fe is six-coordinate. The presence of the substrate triggers Fe coordination changes (**2**) required for O_2 activation and electron transfer from the Rieske cluster (**3**), shown here as an arbitrary Fe-hydroperoxo species. Activated O_2 is utilized productively in the formation of the dihydroxylated product (**4**) or unproductively in the release of reactive oxygen species (ROS).

hardly known.[35] RDOs do not bind the substrate to the non-heme Fe center but require their presence in the substrate binding pocket to induce coordination changes at the non-heme Fe (**1** → **2**, Scheme 1), followed by O_2 binding and electron transfer from the Rieske cluster (**2** → **3**).[30,35] Hydroxylations of aromatic moieties are then carried out by (high-valent) Fe-oxygen species (**3** → **4**) which have been assigned to superoxo-, peroxo-, and oxo species.[32,36−38] While substrates exert some allosteric control on O_2 activation to Fe-oxygen species in RDOs, the substrate is not directly involved in these rate-limiting steps of the catalytic cycle.[31,32,38−40] An assessment of the reactivity of RDOs toward different substrates on the basis of contaminant transformation rates therefore appears somewhat arbitrary.

An often overlooked aspect of catalytic cycles of contaminant-degrading RDOs as well as other O_2 activating enzymes is the unproductive activation of O_2 that generates and releases reactive oxygen species (ROS) from the active site without oxidation of the substrate. Despite being a well-known phenomenon in the activity of non-heme ferrous iron oxygenases,[41−47] this so-called O_2 uncoupling and its consequences for assessing contaminant biotransformation remain largely unexplored (see compilation in Bopp et al.[11]). Uncoupling of activated O_2 can have three principal consequences. First, release of ROS from the active site can be associated with hydroxylation of electron-rich amino acid side chains such as tryptophan and tyrosine residues of the oxygenase itself.[41] Such protein hydroxylations are typically associated with a loss of enzyme activity. Second, a reconfiguration of metabolic fluxes is observed upon ROS release from the oxygenase[48] as part of defense and repair mechanisms of various cell components such as lipids, enzymes, and nucleic acids.[49−51] Qualitatively, such an oxidative stress response has been observed repeatedly in ring-hydroxylating bacteria upon exposure to aromatic compounds[52−54] and involves the consumption of reduction equivalents also used in contaminant oxygenation reactions. Finally, O_2 uncoupling and concomitant formation of ROS have been associated with interferences in the regulation and expression of genes encoding for RDOs, thereby accelerating the enzymatic adaptation toward new substrates.[55−57] Despite the various consequences of O_2 uncoupling on the microbial capability to initiate biodegradation through oxygenation reactions, an understanding of the extent and catalytic mechanism of this process upon exposure of RDOs to different aromatic contaminants is lacking. Given that microbes are exposed to mixtures of organic contaminants in the environment, it would be important to know whether O_2 uncoupling is an innate consequence of the broad substrate specificity of RDOs or whether it is triggered by properties of the substrates that lead, for example, to a bad fit in the active site and ensuing changes in geometric and electronic structures of Fe-oxygen species.[45]

The objective of this work was to evaluate the relevance of O_2 uncoupling for the dioxygenation of aromatic substrates by RDOs and to provide a mechanistic basis to account for this process when assessing contaminant biodegradation. Here, we studied two important and well-characterized nitroarene dioxygenases, 2-nitrotoluene dioxygenase (2NTDO) and nitrobenzene dioxygenase (NBDO), as representative RDOs.[40,58−64] We obtained insights into the substrate- and enzyme-specificity of O_2 uncoupling in a comprehensive evaluation of the activity of 2NTDO as well as through extension of a previous data set for NBDO.[65] The specific goals were as follows. (1) We aimed to quantify the extent of O_2 uncoupling for a wide set of structurally related substrates of nitroarene dioxygenases on the basis of in vitro enzyme assays. 2NTDO and NBDO share 95% sequence identity and cover a similar substrate spectrum,[64] yet two distinct active site residues have been found to alter the enzymes' substrate specificity.[66] (2) We elucidated the catalytic mechanism of nitroarene dioxygenases to characterize the elementary reactions responsible for O_2 uncoupling by RDOs. To that end, we studied kinetic isotope effects of both substrates, O_2 and nitroaromatic compounds, to probe for the mechanisms and timing of their reactions in the catalytic cycle. While ^{18}O kinetic isotope effects (^{18}O-KIEs) were used to infer the type of reactive Fe-oxygen species formed,[67−73] ^{13}C-KIEs allowed for studying the initial step of aromatic hydroxylation.[40,61,74] (3) We examined the influence of substrate molecular structure on the oxygenation reaction by comparing the extent of O_2 uncoupling for a broad set of methylated, hydroxylated, fluorinated, and chlorinated nitroaromatic substrates. Finally, we rationalize wider implications of O_2 uncoupling scrutinized here for two RDOs for assessing oxidative contaminant biodegradation in the environment.

EXPERIMENTAL SECTION

All chemicals and material used are reported in section S1 in the Supporting Information (SI). Enzyme purification procedures were largely adapted from previous works[60,75,76] as described in section S2. Experimental procedures follow methods described by Pati and co-workers[61,65] and are summarized in the following.

Enzyme Assays

Controlled Substrate Turnover Experiments. We quantified the turnover of nitroaromatic substrates to organic and inorganic reaction products (substituted catechols, benzylic alcohols, and nitrite)

https://doi.org/10.1021/acsenvironau.2c00023
ACS Environ. Au 2022, 2, 428−440

as well as O_2 disappearance from a single set of enzyme assays where the reaction progress was controlled through the amount of NADH added. The same samples were also used for determination of organic substrate $^{13}C/^{12}C$ and $^{18}O/^{16}O$ ratios of dissolved O_2. Due to the amounts of O_2 required for $^{18}O/^{16}O$ ratio measurements in gaseous O_2,[77,78] these assays were set up in 12 mL clear-glass crimp-top vials. Each vial contained a magnetic stir bar and was filled completely (i.e., without headspace) and closed with butyl rubber aluminum crimp seals. Experiments were carried out in 50 mM MES buffer (pH 6.8) equilibrated at room temperature (20−25 °C) to obtain initial dissolved O_2 concentrations of 220−280 μM. Assays consisted of 0.15 μM reductase, 1.8 μM ferredoxin, 0.15 μM oxygenase, 100 μM $(NH_4)_2Fe(SO_4)_2$, and 40−170 μM nitroaromatic substrate added from 50 mM methanolic stock solutions. Purified oxygenase was thawed directly before the experiment, whereas ferredoxin and reductase were kept in the refrigerator for up to 1 week. Reactions were initiated by the addition of 10−50 μL of 50 mM NADH stock (in 10 mM NaOH) with a gastight glass syringe through the septum of the closed vials. NADH concentrations of stock solutions were determined spectrophotometrically ($\epsilon_{340\ nm}$= 6300 L mol^{-1} cm^{-1}).[79] For each enzyme−substrate combination, four to six replicate experiments, each with a different initial NADH concentration (20−330 μM), were performed in separate reactors. Dissolved O_2 concentrations were monitored continuously with a needle-type oxygen microsensor (PreSens, Precision Sensing GmbH) immersed into the assay under constant stirring of the sample at 300 rpm. Reactions were run until complete oxidation of NADH which became evident from spectrophotometric measurements of NADH as well as from the observation of O_2 concentration leveling off at constant concentrations after 5−40 min. Initial nitroaromatic substrate concentrations were determined in sample vials with substrate in MES buffer in the absence of any enzyme. Background consumption of O_2 in enzyme assays was monitored and assessed systematically as described in section S3.1.

Quantification of H_2O_2. We quantified H_2O_2 formation for a selected number of enzyme−substrate combinations in separate enzyme assays where horse radish peroxidase (HRP) was used to catalyze the reduction of H_2O_2 with concomitant oxidation of 4-methoxyaniline or 10-acetyl-3,7-dihydroxyphenoxazine (Ampliflu).[80,81] Losses of 4-methoxyaniline or Ampliflu provided a measure for the amount of H_2O_2 formed.

In assays with NBDO and 2- and 4-nitrotoluene, H_2O_2 was quantified from aliquots of controlled turnover assay described above. After complete NADH oxidation, 900 μL aliquots were withdrawn and mixed with 100 μL of an HRP assay in MES buffer resulting in final concentrations of 10 mg L^{-1} HRP and 500 μM 4-methoxyaniline. 4-Methoxyaniline consumption was quantified on HPLC as described in section S3.2.1 and an external calibration row of 4-methoxyaniline consumption by HRP with a range of H_2O_2 concentrations of 50−250 μM.

For experiments with 2NTDO, we prepared separate assays for the quantification of H_2O_2 formation with nitrobenzene, 2-nitrotoluene, as well as the three chloronitrobenzene isomers. The assays were prepared in 2 mL crimp vials filled completely with MES buffer containing 0.15 μM reductase, 1.8 μM ferredoxin, 0.15 μM oxygenase, 100 μM $(NH_4)_2Fe(SO_4)_2$, and 300 μM of nitroaromatic substrate. Substrate oxygenations were initiated by addition of 100−200 μM of NADH through the septum and run with continuous stirring and O_2 monitoring until O_2 concentrations remained constant. Subsequently, 900 μL aliquots were mixed with 100 μL of the above-mentioned HRP assay in MES buffer (10 mg L^{-1} HRP and 400 μM Ampliflu). Ampliflu was quantified spectrophotometrically at 560 nm on a plate reader (Synergy Mx, Biotek Instruments Inc., Vermont, VT, USA) and an external calibration row of Ampliflu with a range of H_2O_2 concentrations from 20 to 250 μM.[80]

Kinetics of Enzymatic O_2 Consumption. The kinetics of O_2 consumption were determined in 2 mL crimp vials equipped with a magnetic stir bar (300 rpm) at approximately 22 °C and filled completely with enzyme assay solution following procedures established by Pati et al.[65] All assays contained slightly modified concentrations to prevent anything but O_2 availability limiting turnover (0.3 μM reductase, 3.6 μM ferredoxin, 0.15 μM oxygenase, 500 μM $(NH_4)_2Fe(SO_4)_2$), and experiments were run in excess of nitroaromatic substrate (500 μM). Reactions were initiated through the addition of NADH from a 100 mM stock solution through the septum to obtain a final concentration of 1000 μM. All experiments were run until complete consumption of dissolved O_2 (250 μM).

Substrate Oxygenation Kinetics from NO_2^- Formation. The initial rates of NO_2^- formation from nitrobenzene, 2-nitrotoluene, and 3-chloronitrobenzene were determined in triplicate at six different initial substrate concentrations ranging from 10 to 300 μM. Experiments were performed at room temperature (approximately 20 °C) in 1.5 mL plastic tubes containing 0.5 mL of MES buffer (50 mM, pH 6.8) with 0.3 μM reductase, 3.6 μM ferredoxin, 0.15 μM oxygenase, and 500 μM $(NH_4)_2Fe(SO_4)_2$. The reaction was initiated by the addition of 500 μM NADH, and 100 μL samples were withdrawn after 20, 30, 40, and 50 s. The reaction was quenched with 200 μL of sulfanilamide (10 g L^{-1} in 1.5 M HCl) followed by the addition of 200 μL of *N*-(1-naphthyl)ethylenediamine dihydrochloride (1 g L^{-1} in 1.5 M HCl). NO_2^- was quantified using a photometric method at 540 nm[82] with an external calibration exhibiting standard deviations of <3 μM.

Chemical and Isotopic Analyses

Quantification of Organic Substrate and Product Concentrations. Organic substrates, nitrobenzylalcohols, and catecholic products were quantified by HPLC as described in detail in section S3.2.1.

Stable Isotope Analyses. After completion of controlled substrate turnover experiments, the 12 mL vials were prepared for analysis of $^{18}O/^{16}O$ ratios in O_2 according to procedures described previously.[61,77,78] Briefly, 3 mL of the assay solution was removed with a gastight syringe by simultaneously filling the vial with N_2 gas (5.0) at a constant pressure of 2 bar. The reactors were placed upside down on an orbital shaker at 200 rpm for 30 min to accelerate partitioning of O_2 into the headspace. Then 1000 μL of gaseous headspace was injected into a gas chromatograph coupled via a Conflo IV interface to an isotope ratio mass spectrometer (GC/IRMS, Thermo Fisher Scientific). Duplicate injections of three samples were bracketed by three injections of ambient air that served as a reference standard for $\delta^{18}O$ values reported vs Vienna Standard Mean Ocean Water (VSMOW). The $\delta^{18}O$ values of the reference gas was calibrated with O_2 signals from on-column injections of air assuming a constant $\delta^{18}O_{air}$ of 23.88‰.[83] Instrument parameters were reproduced according to Bopp et al.[78] with either two connected PLOT columns (Restek from BGB Analytik; 30 m × 0.32 mm ID, 30 μ m film thickness) or a single column employing a linear correction factor to exclude Ar interference in the measurement of $^{18}O/^{16}O$ isotope ratios. Each sequence included three blank samples of O_2-free water that was obtained from 20 min of purging under a constant stream of N_2 and treated similarly to the samples to account for diffusive O_2 contamination.[84]

Carbon isotope ratios ($^{13}C/^{12}C$) of organic substrates were determined from the 3 mL aqueous samples withdrawn from the 12 mL vials for generation of the N_2 headspace. Nitroaromatic compounds were extracted from aqueous samples by solid phase microextraction (SPME) and analyzed for $^{13}C/^{12}C$ ratios on a GC/IRMS equipped with a GC combustion III interface. Instrumental procedures were described in detail in refs 40 and 61. Samples were diluted to substrate concentrations that resulted in constant peak amplitudes between 0.5 and 8 V. Triplicate measurements of three samples were bracketed by three injections of calibrated in-house reference materials spanning $\delta^{13}C$ values between −55‰ and +7.7‰ to ensure accuracy of the measurements. $\delta^{13}C$ values are reported relative to Vienna PeeDee Belemnite ($\delta^{13}C_{VPDB}$).

Data Evaluation

Reaction Stoichiometries. Reaction stoichiometries of substrate consumption and product formation were normalized to the amount of external reduction equivalents (NADH) of five to eight replicate experiments. Stoichiometric coefficients of species j, $|\nu_j|$, were calculated through linear regressions of eq 1 for the different concentrations of nitroaromatic substrate, dissolved O_2, hydroxylated aromatic product,

https://doi.org/10.1021/acsenvironau.2c00023
ACS Environ. Au 2022, 2, 428−440

and NO_2^- obtained from experiments with different amounts of added NADH.

$$[j] = v_j \times [\mathrm{NADH}] + q \quad (1)$$

where $[j]$ is the measured molar concentration of substrate, dissolved O_2, hydroxylated organic product, or nitrite at the end of an experiment, [NADH] is the nominal concentration of NADH, and q is the y-intercept (Figure 1). Uncertainties of $|v_j|$ reflect errors arising from linear regression analysis and are reported as 95% confidence intervals.

The extent of O_2 uncoupling, $f_{O_2\text{-uc}}$, was calculated through linear regressions of eq 2:

$$[NO_2^-] + [\mathrm{NBA}] = (1 - f_{O_2\text{-uc}})([O_2]_0 - [O_2]) + b \quad (2)$$

where $[NO_2^-]$ is the concentration of nitrite formed, $[O_2]_0$ is the initial O_2 concentration, $[O_2]$ is the residual O_2 concentration, and [NBA] is the concentration of nitrobenzylalcohol formed by monooxygenation. Figure S3 illustrates regressions for the derivation of O_2 uncoupling for substrates with efficient and inefficient oxygenation of 2-nitrotoluene and 4-chloronitrobenzene, respectively. Procedures for evaluation of and accounting for background consumption of O_2 in enzyme assays are documented in section S3.1.

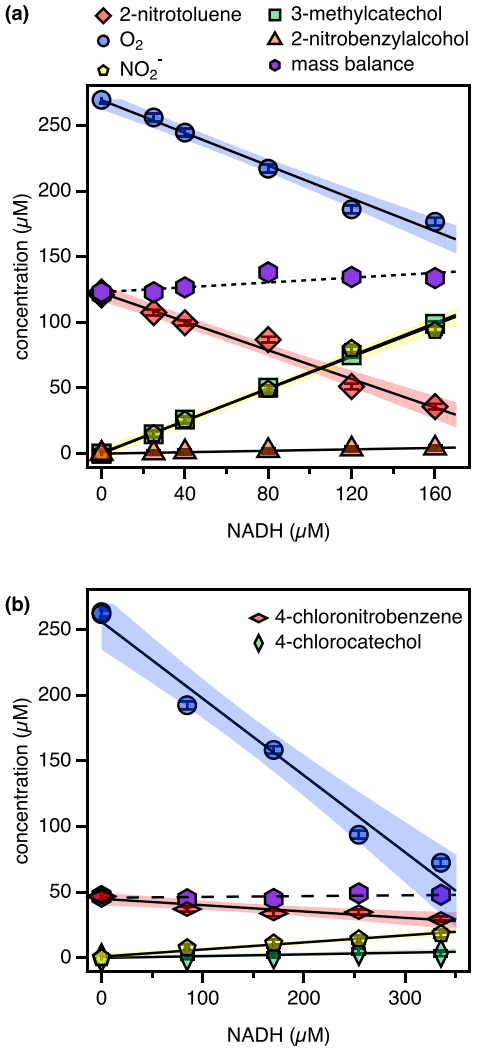

Figure 1. Concentrations of substrate, dissolved O_2, organic products, and NO_2^- in 2NTDO assays after complete consumption of different amounts of NADH. The black lines and shaded areas represent linear fits with 95% confidence intervals with slopes shown in Table S4. With 2-nitrotoluene as the substrate (a), the mass balance represents the concentrations of 2-nitrotoluene, NO_2^-, and 2-nitrobenzylalcohol. For 4-chloronitrobenzene (CNB) as the substrate (b), the mass balance represents the concentrations of 4-chloronitrobenzene and NO_2^-.

Isotope Effects. Apparent kinetic isotope effects pertinent to the hydroxylation of aromatic carbon, ^{13}C-KIE, were derived from nonlinear correlations of fractional amount of residual substrate vs the observable changes in $^{13}C/^{12}C$ ratios and are expressed in terms of C isotope signatures, $\delta^{13}C$, and C isotope enrichment factors, ϵ_C, according to eqs 3 and 4.

$$\frac{\delta^{13}C + 1}{\delta^{13}C_0 + 1} = \left(\frac{[S]}{[S]_0}\right)^{\epsilon_C} \quad (3)$$

$$^{13}\text{C-KIE} = \frac{1}{1 + n_C\epsilon_C} \quad (4)$$

where $\delta^{13}C$ and $\delta^{13}C_0$ are the C isotope signatures of the substrate in an experiment vs its original value, respectively. [S] and $[S]_0$ are the residual and initial substrate concentrations, respectively. n_C is the number of carbon atoms in the substrate, which accounts for the isotopic dilution of the isotope effect based on the assumption of an asynchronous hydroxylation mechanism.[31,61] Nonlinear regression fit weighted with the standard deviation of triplicate measurements were carried out in Igor Pro (WaveMetric Inc.). Note that in cases of substantial O_2 uncoupling, when substrate turnover was below 30% and changes in $\delta^{13}C$ of the substrates remained within the total uncertainty of $^{13}C/^{12}C$ ratio measurements of 0.5‰, ^{13}C-KIE were set to unity (section S3.4).

Kinetic isotope effects associated with O_2 activation by nitroarene dioxygenases, ^{18}O-KIE, were derived as average for both O_2 atoms in O_2 according to eq 5 following the identical procedures as outlined above.

$$\frac{\delta^{18}O + 1}{\delta^{18}O_0 + 1} = \left(\frac{[O_2]}{[O_2]_0}\right)^{1/^{18}\text{O-KIE}-1} \quad (5)$$

where $[O_2]$ and $[O_2]_0$ are the residual and initial dissolved O_2 concentrations, respectively.

RESULTS AND DISCUSSION

Efficiency of Substrate Oxygenation by 2-Nitrotoluene Dioxygenase

2-Nitrotoluene dioxygenase carries out hydroxylations of nitroaromatic substrates with the concomitant oxidation of NADH for O_2 activation.[64] Like other nitroarene dioxygenases, 2NTDO catalyzes the dioxygenation of the aromatic moiety to *cis*-dihydroxylated intermediates that spontaneously form catecholic products and NO_2^- (Scheme 2). To a lesser extent, the methyl group of nitrotoluene undergoes monooxygenation forming nitrobenzylalcohols.

Figure 1a shows substrate consumption and product formation for 2-nitrotoluene at different extents of turnover according to the concentration of NADH provided. 2-Nitro-

Scheme 2. Reactions Catalyzed by 2-Nitrotoluene Dioxygenase

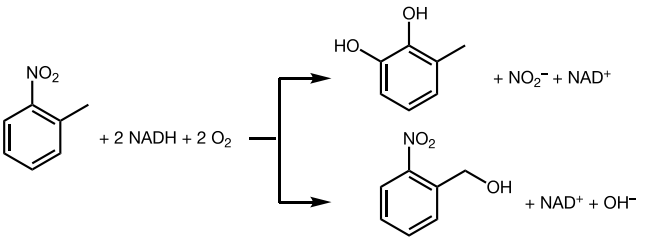

https://doi.org/10.1021/acsenvironau.2c00023
ACS Environ. Au 2022, 2, 428−440

Table 1. Stoichiometries for O_2 Activation and Dioxygenation of Substituted Nitroaromatic Substrates by 2NTDO and NBDO as well as the ^{13}C-KIE and ^{18}O-KIE Values of the Substrates[a]

entry	(co)substrate	υ_j[b]	$f_{O_2\text{-uc}}$[c]	^{18}O-KIE	^{13}C-KIE
2NTDO					
1a	nitrobenzene	0.50 ± 0.02	0.33 ± 0.02		1.007 ± 0.001
1b	O_2 (NB)	0.65 ± 0.01[d]		1.015 ± 0.001	
2a	2-nitrotoluene	0.62 ± 0.02	0.02 ± 0.03		1.006 ± 0.002
2b	O_2 (2-NT)	0.63 ± 0.01[d]		1.016 ± 0.002	
3a	3-nitrotoluene	0.16 ± 0.02	0.84 ± 0.03		1.004 ± 0.001
3b	O_2 (3-NT)	0.99 ± 0.01		1.018 ± 0.001	
4a	4-nitrotoluene	0.05 ± 0.01	0.94 ± 0.01		1.003 ± 0.001[e]
4b	O_2 (4-NT)	0.85 ± 0.01		1.021 ± 0.003	
5a	2-fluoronitrobenzene	0.40 ± 0.02	0.36 ± 0.03		1.002 ± 0.004
5b	O_2 (2-F-NB)	0.68 ± 0.01[d]		1.015 ± 0.001	
6a	3-fluoronitrobenzene	0.44 ± 0.03	0.35 ± 0.07		1.011 ± 0.006
6b	O_2 (3-F-NB)	0.62 ± 0.01[d]		1.016 ± 0.001	
7a	4-fluoronitrobenzene	0.13 ± 0.01	0.83 ± 0.01		1.005 ± 0.001
7b	O_2 (4-F-NB)	0.79 ± 0.01		1.019 ± 0.001	
8a	2-chloronitrobenzene	0.66 ± 0.05	0.21 ± 0.05		0.998 ± 0.002
8b	O_2 (2-Cl-NB)	0.79 ± 0.01[d]		1.015 ± 0.001	
9a	3-chloronitrobenzene	0.10 ± 0.01	0.79 ± 0.02		1.011 ± 0.001
9b	O_2 (3-Cl-NB)	0.51 ± 0.01[d]		1.016 ± 0.001	
10a	4-chloronitrobenzene	0.04 ± 0.01	0.92 ± 0.01		1.007 ± 0.006
10b	O_2 (4-Cl-NB)	0.59 ± 0.01		1.013 ± 0.001	
11a	2-nitrophenol	0.07 ± 0.01	0.94 ± 0.01		1.000[f]
11b	O_2 (2-NP)	1.09 ± 0.01[d]		1.014 ± 0.001	
12	O_2 (3-nitrophenol)	1.07 ± 0.01	1.00[g]	1.015 ± 0.001	
13a	4-nitrophenol	0.04 ± 0.01	0.94 ± 0.01		1.000[f]
13b	O_2 (4-NP)	0.80 ± 0.01		1.016 ± 0.001	
NBDO					
14a	2-nitrotoluene	0.18 ± 0.02	0.62 ± 0.01		1.018 ± 0.001[h]
14b	O_2 (2-NT)	0.89 ± 0.01		1.018 ± 0.001	
15a	4-nitrotoluene	0.18 ± 0.02	0.74 ± 0.01		1.010 ± 0.001[h]
15b	O_2 (4-NT)	0.80 ± 0.01		1.013 ± 0.001	

[a]Uncertainties correspond to 95% confidence intervals. [b]NADH-normalized stoichiometry of (co)substrate consumption calculated with eq 1; substrate dihydroxylation is quantified on the basis of measured NO_2^- concentrations. [c]O_2 uncoupling determined with eq 2. [d]Without O_2 background consumption according to eq S2. [e]Reproduced from Pati et al.[40] due to low turnover; see section S3.4. [f]^{13}C-KIE set to unity; see section S3.4. [g]No NO_2^- detected. [h]reproduced from Pati et al.[40] excluding monooxygenation with kinetic model.[60]

toluene is transformed almost exclusively to 3-methylcatechol and equivalent amounts of NO_2^- with the generation of only minor traces of 2-nitrobenzylalcohol. The mass balance of organic substrate and products confirms that 2NTDO carried out the two hypothesized hydroxylation reactions. The stoichiometric coefficients of substrate loss and product formation normalized to the amounts of NADH added, υ_j, from Tables 1 and S7 allow for an assessment of the oxygenation efficiency of 2NTDO with 2-nitrobenzene. The O_2 consumption coefficient, υ_{O_2}, of 0.63 ± 0.01 mol/mol of NADH illustrates that some reduction equivalents of NADH were not involved in O_2 activation by 2NTDO in this experiment series (section S4.3 and Table S4). 3-Methylcatechol and 2-nitrobenzylalcohol were formed at 0.62 ± 0.02 and 0.03 ± 0.01 mol/mol NADH, respectively. Detection of both dioxygenation products, 3-methylcatechol and NO_2^-, at equal stoichiometries ($\upsilon_{NO_2^-}$ = 0.63 ± 0.06) confirmed the accuracy of our analytical procedures and thus allowed for quantifying the dioxygenation reactions in Table 1 on the basis of NO_2^- measurements.[61,65] The stoichiometric coefficient for O_2 consumption is identical within uncertainty, implying that all activated O_2 is used in hydroxylation reactions. Accordingly, we did not observe any O_2 uncoupling ($f_{O_2\text{-uc}}$ = 0.02 ± 0.03, Table 1, entry 2).

In contrast to the case of 2-nitrotoluene, 2NTDO hydroxylated other substrates very inefficiently. Figure 1b shows the results of a substrate turnover experiment for 4-chloronitrobenzene. Coefficients for substrate consumption, υ_S, and dioxygenation, $\upsilon_{NO_2^-}$, are small and identical at 0.04 mol/mol NADH, whereas O_2 consumption is substantially higher (υ_{O_2} = 0.59 ± 0.01 mol/mol NADH, Table 1, entries 10a/b). Thus, only 8% of O_2 consumption was utilized for substrate hydroxylation, whereas the remaining 92% led to unproductive O_2 activation. We recovered up to 43% of the consumed O_2 as H_2O_2 in additional assays (Table S6), confirming not only that a large fraction of the uncoupled O_2 was present as ROS but also that these species were released into solution. The comparison of these data for 2-nitrotoluene and 4-chloronitrobenzene furthermore shows that the efficiency of oxygenation vs O_2 uncoupling is highly variable.

We systematically evaluated this substrate dependence of O_2 uncoupling by 2NTDO for a broad range of structurally related compounds. All nitroaromatic substrates led to O_2 consumption that exceeded the background O_2 disappearance at 3 μM min^{-1}

https://doi.org/10.1021/acsenvironau.2c00023
ACS Environ. Au 2022, 2, 428−440

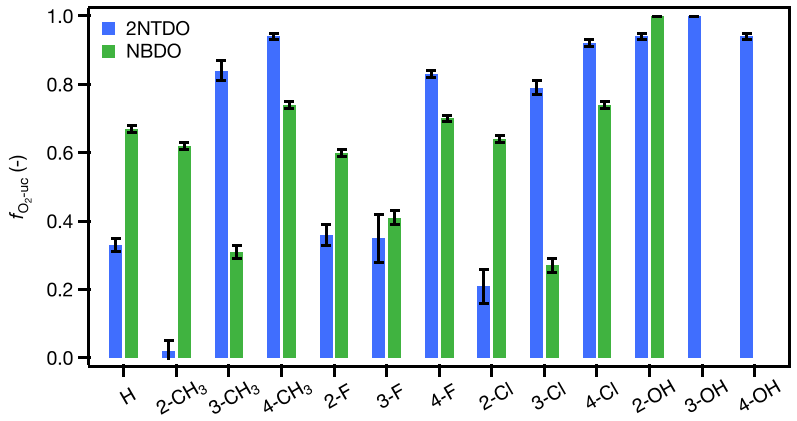

Figure 2. Extent of O_2 uncoupling in 2-nitrotoluene dioxygenase (blue, 2NTDO) and nitrobenzene dioxygenase (green, NBDO[65]) with substituted nitrobenzenes (data from Table 1).

Scheme 3. Catalytic Cycle of the Dioxygenation of Nitroaromatic Substrates by 2NTDO and NBDO Based on Studies of NDO and NBDO[39,65a]

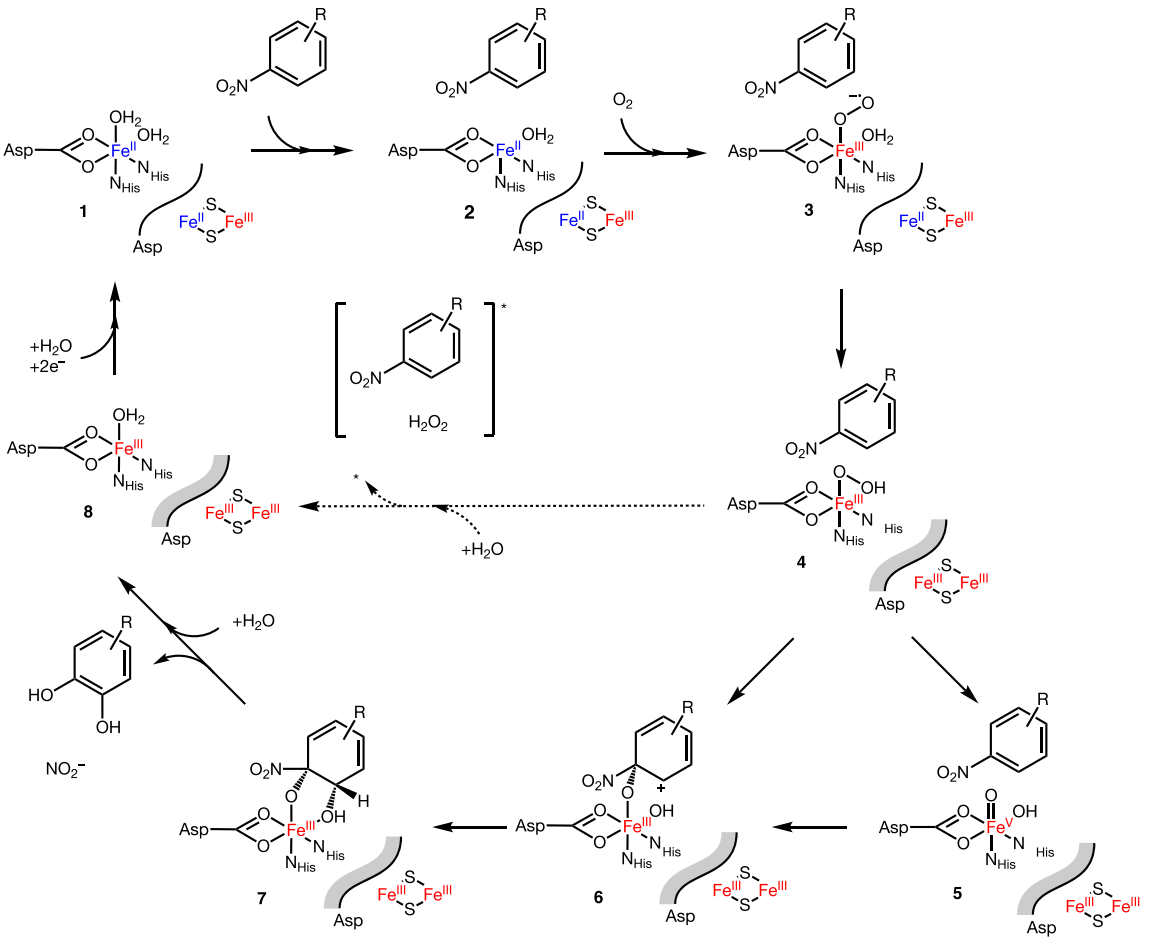

[a]Illustration shows the non-heme Fe^{II} active site, a generic nitroaromatic substrate, and the [2Fe-2S] Rieske cluster in different oxidation states.

by at least 3-fold (Figures S1 and S5) whereas non-nitrated compounds, such as benzene or toluene, did not cause any O_2 disappearance beyond the background rate (section S4.1). Figure 2 shows $f_{O_2\text{-uc}}$ values for nitrobenzene as well as methylated, fluorinated, chlorinated, and hydroxylated nitrobenzenes used as model compounds to study the effects of substrate molecular structure on nitroarene activities. Many of these compounds are known environmental contaminants that can undergo oxidative biodegradation.[85−89] With exception of 2-nitrotoluene, all substrates lead to substantial O_2 uncoupling and this unproductive path of O_2 activation even predominated enzymatic activity. The type of aromatic substituent is largely

https://doi.org/10.1021/acsenvironau.2c00023
ACS Environ. Au 2022, 2, 428−440

irrelevant for the extent of hydroxylation vs O_2 uncoupling. In assays containing chlorinated nitrobenzene, for example, $f_{O_2\text{-uc}}$ ranged from 20% to 90% (entries 8−10, Table 1). Nitrophenols exclusively promoted unproductive O_2 activation ($f_{O_2\text{-uc}} > 0.9$).

Figure 2 also shows the O_2 uncoupling activity of NBDO with data from Pati et al.[65] Compared to 2NTDO, $f_{O_2\text{-uc}}$ values for NBDO were confined to a smaller range of values between 0.31 ± 0.02 (3-nitrotoluene) and 0.74 ± 0.01 (4-chloronitrobenzene). Nitrophenol was not hydroxylated by NBDO, similarly to what was found for 2NTDO. NBDO and 2NTDO also show very distinct substrate specificity. 2-Chloronitrobenzene, for example, differs in $f_{O_2\text{-uc}}$ values by 43% between assays of 2NTDO vs NBDO. Only one substrate, 3-fluoronitrobenzene, exhibited the extent of O_2 uncoupling within <10% for both NBDO and 2NTDO. It is interesting to note that the eponymous and thus potentially optimized substrate for dioxygenation by 2NTDO, 2-nitrotoluene, lacks O_2 uncoupling whereas NBDO shows a poor oxygenation efficiency with nitrobenzene as substrate ($f_{O_2\text{-uc}} = 0.67 \pm 0.01$). A more detailed discussion of the substrate-specific impacts on $f_{O_2\text{-uc}}$ values follows below.

O_2 Uncoupling in the Catalytic Cycle of Nitroarene Dioxygenases

We analyzed the catalytic cycle of nitroarene dioxygenases outlined in Scheme 3 for possible O_2 uncoupling reactions by dissecting the rate-limiting steps leading to the consumption of O_2 and the aromatic substrate. To that end, we quantified ^{18}O-KIEs for O_2 activation in Fe-oxygen species according to the methodology applied previously to study O_2 activating processes in non-heme ferrous iron oxygenases.[65,67,68,70−72,90] ^{13}C-KIEs were used to characterize the timing of substrate hydroxylation. The corresponding data are compiled in Table 1.

Rate-Limiting Steps of O_2 Activation. We derived the ^{18}O-KIEs of O_2 by 2NTDO for the entire set of nitroaromatic substrates by evaluating changes in $^{18}O/^{16}O$ ratios of the residual dissolved O_2 at different extents of turnover (Figure 3a). We observed moderately large O isotope fractionation which followed the trends described in eq 5. All ^{18}O-KIEs were confined to values between 1.013 and 1.020 (Table 1) with an average value of 1.016, and they are thus independent of the elementary reaction step leading to O_2 uncoupling (Figure 3b). This observation strongly suggests the formation of one type of Fe-oxygen species regardless of the nitroaromatic substrate. Comparison of experimental ^{18}O-KIE values with theoretical ^{18}O equilibrium isotope effects (^{18}O-EIEs) of Mirica et al.[68] imply the formation of ferric iron (hydro)peroxo species (Fe^{III}−OO(H), ^{18}O-EIE of 1.0172), a species that has previously been postulated to catalyze oxygenations by naphthalene dioxygenase.[31,37] Smaller ^{18}O-KIE values, by contrast, stand for Fe-superoxo species (^{18}O-EIE of 1.0080), whereas higher ^{18}O-KIE have been assigned to Fe^{IV}═O (^{18}O-EIE of 1.0287).[68]

The observation of a narrowly confined ^{18}O-KIE for O_2 activation by 2NTDO is consistent with data obtained for NBDO[65] and suggests that the two nitroarene dioxygenases follow the same initial catalytic mechanism. As shown in Scheme 3 in reactions **1** → **2** → **3** → **4**, the presence of substrate in the active site induces the loss of a H_2O ligand at the non-heme Fe (**2**) followed by O_2 binding and activation (**3**). Substrate binding ultimately promotes the electron transfer from the Rieske cluster (Fe^{II}−Fe^{III} → Fe^{III}−Fe^{III} in **3** → **4**) that enables

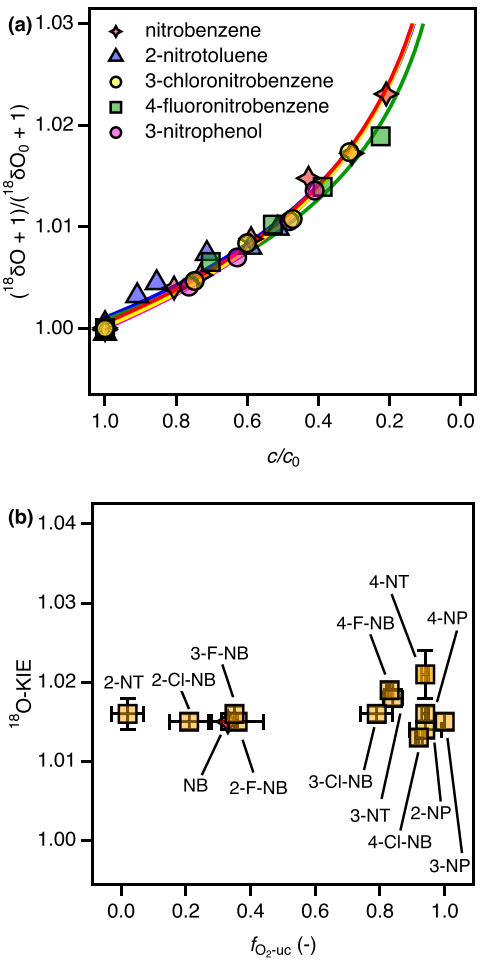

Figure 3. Changes of $^{18}O/^{16}O$ ratios (a) and ^{18}O-KIE of O_2 activation (b) by 2NTDO in the presence of various substrates.

generation of the ferric Fe-(hydro)peroxo species (**4**) in the rate-limiting step of O_2 consumption. A common mechanism of O_2 activation in nitroarenes confirms the widely made observation that the kinetics of O_2 activation are triggered by the substrate but do not involve interactions of the substrate with the non-heme Fe species.[35] It follows from the conserved ^{18}O-KIE values that the substantial substrate-dependence of O_2 uncoupling must originate from reaction steps after generation of species **4**.

A number of observations suggest that O_2 uncoupling would happen primarily from species **4**. Previous works with NBDO have shown that the first step of the asynchronous hydroxylation of the substrate (**4** → **5** or **4** → **6**) is irreversible.[38,40] O_2 uncoupling therefore has to occur from **4** or **5**. This conclusion is supported by the fact that the substrate has to be released in an unreacted form, in agreement with the mass balances of aromatic compounds illustrated above (Figure 1). Finally, we detect a large share of the uncoupled O_2 as H_2O_2 in the assay solutions. As shown in Table S6, H_2O_2 concentrations do not account for all of the uncoupled O_2, suggesting that some H_2O_2 could have reacted further with electron rich moieties within the proteins or the buffer. We rule out a release of superoxide from species **3** given that this process would need to occur reversibly to be consistent with the ^{18}O-KIEs. O_2 uncoupling from species **5**, on the other hand, is an unlikely source of H_2O_2 because the cleavage of O−O bonds is typically irreversible.[70] The most likely reaction of **5** with concomitant loss of O_2 is a

https://doi.org/10.1021/acsenvironau.2c00023
ACS Environ. Au 2022, 2, 428−440

monooxygenation reaction with nitrotoluene substrates in which the release of reduced oxygen would occur as H_2O.[65]

Timing of Substrate Hydroxylation. The ^{13}C-KIE values in the 12 reactive substrates were derived from the C isotope fractionation as shown in Figure S7 on the basis of eqs 3 and 4. Note that due to the low turnover of many substrates, their carbon isotope fractionation is difficult to detect (see discussion in section S3.4). All ^{13}C-KIE values are small, vary between unity and 1.01 (Table 1), and are not correlated with O_2 uncoupling as shown in Figure 4a. These values are notably smaller than experimentally observed and theoretically derived intrinsic ^{13}C-KIEs which can be as large as 1.024 and 1.039, respectively.[40,86] The observation of small isotope fractionation after the rate-limiting step of the catalytic cycle (i.e., O_2 activation) is nevertheless counterintuitive. Such kinetic mechanisms typically show a complete absence of substrate isotope fractionation as shown for flavin-dependent oxygenases.[74] We posit that the observed C isotope fractionation and the nonunity of ^{13}C-KIEs associated with the activity of 2NTDO are due to the O_2 uncoupling process and reflect the reaction path **4** → **5** → **6**. This path is also distinct from the one postulated previously for NBDO.[65] To observe C isotope fractionation in the unreacted substrate released through uncoupling from species **4**, the following reactions would need to involve isotope-sensitive bonding changes and be reversible. While hydroxylations of aromatic carbon in reaction **5** → **6** fulfils the first requirement with a large intrinsic ^{13}C-KIE for the formation of the Fe^{V}-(oxo)hydroxo species,[40] reaction **4** → **5** is presumably not reversible for reasons outlined above. To that end, C isotope fractionation from the hydroxylation does not alter the $^{13}C/^{12}C$ ratio of the nitroaromatic substrate in species **4** that could be observed upon O_2 uncoupling. Indirect confirmation for this interpretation comes from comparison of the identical type of data for NBDO in Figure 4b.[65] In this case, the progressive expression of a ^{13}C-KIE with increasing $f_{O_2\text{-uc}}$ values is due to a partly reversible reaction **4** → **6** which alters the $^{13}C/^{12}C$ ratio of the remaining substrate. The substrate C isotope fractionation observed therefore increases with increasing extent of O_2 uncoupling.

Effect of Substrate Structure and Active Site Residues on O_2 Uncoupling

We evaluated the consequences of structural factors pertinent to substrate substituent types and positions as well as the enzyme's active site to elucidate possible causes for the distinct substrate specificity and O_2 uncoupling behavior shown in Figure 5. 2NTDO and NBDO share 95% sequence identity and differ

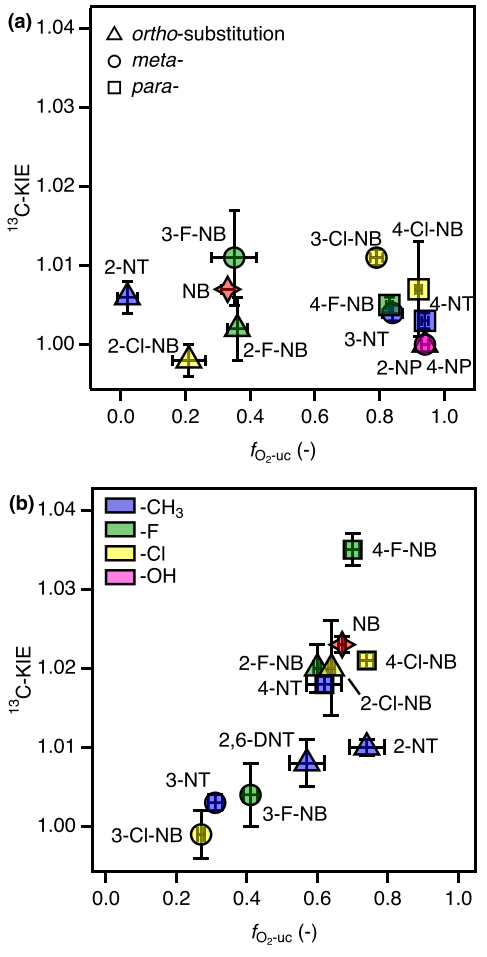

Figure 4. ^{13}C-KIEs of substrate dioxygenation by 2NTDO (a) and NBDO (b) vs fraction of uncoupled O_2 activation, $f_{O_2\text{-uc}}$. Panel (b) was constructed with data from Pati et al.[65] and this study.

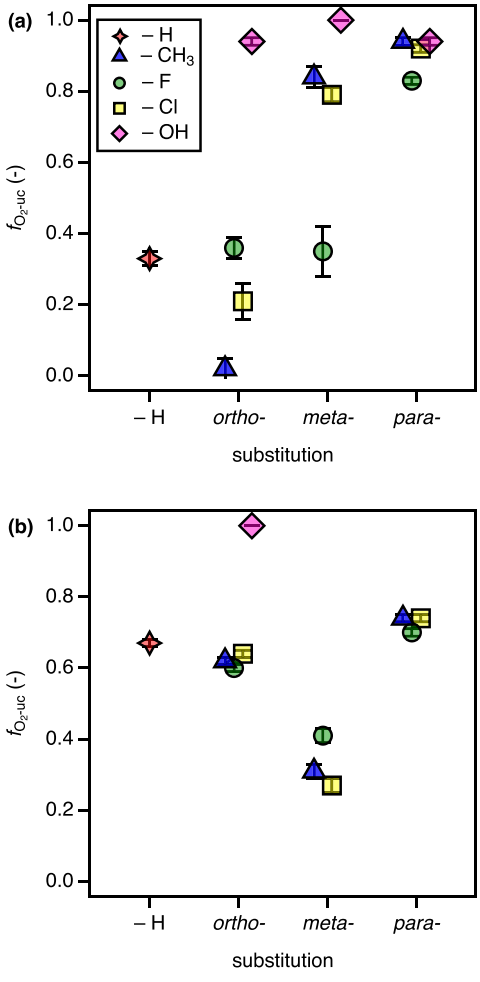

Figure 5. Extent of O_2 uncoupling, $f_{O_2\text{-uc}}$, caused by different substituted nitrobenzenes in 2NTDO (a) and NBDO (b) vs position of the aromatic substituent of the substrate. The legend in panel (a) applies to both figures.

https://doi.org/10.1021/acsenvironau.2c00023
ACS Environ. Au 2022, 2, 428−440

only slightly in their active site residues.[64] While both enzymes exhibit the Asn258 residue responsible for H-bonding to the oxygen atoms of the nitro group, 2NTDO hosts an Ile residue at position 293 where NBDO has a more bulky Phe. This additional space in the active site of 2NTDO was hypothesized to allow for a favorable binding of 2-nitrotoluene so that the aromatic ring is oriented toward the reactive Fe-oxygen species for dioxygenation despite its *ortho*-methyl substituent.[64] In fact, we observed a reduced O_2 uncoupling for 2NTDO with 2-nitrotoluene and other *ortho*-substituted substrates (Figure 5a). Nitrophenol substrates are not discussed further because these compounds are not dioxygenated by any of the two enzymes. Based on this reasoning, the increased $f_{O_2\text{-uc}}$ values for chlorine and methyl substituents in *meta*- and any substituent in *para*-position can be explained by a poor substrate fit in the active site as primary origin of O_2 uncoupling. This interpretation is also supported qualitatively by the relatively lower $f_{O_2\text{-uc}}$ values for nitrobenzene and, given the smaller size of fluorine, for 3-fluorobenzene.

We observed distinct trends for $f_{O_2\text{-uc}}$ values in NBDO (Figure 5b). Here, the eponymous substrate nitrobenzene exhibits a relatively high extent of O_2 uncoupling of about 60% which is also found for *ortho*- and *para*-substituted nitrobenzenes. By contrast, *meta*-substitution with $-CH_3$, $-F$, and $-Cl$ allowed for a more efficient dioxygenation of the substrates. The finding that $f_{O_2\text{-uc}}$ values for the methyl-, fluoro-, and chloro-substituted nitrobenzenes with NBDO cluster together reinforces the interpretation of data for 2NTDO that the structure of the substrate is a likely determinant of O_2 uncoupling. At first sight, electronic effects appear to be of negligible relevance even though $-CH_3$ vs halogen substituents alter the partial atomic charges of the C atoms and thus the susceptibility for attack by electrophilic Fe-oxygen species in RDOs.[32]

None of the trends revealed in Figure 5, however, allows one to rationalize the preference of 2NTDO and NBDO for oxygenation of *ortho*- and *meta*-substituted nitrobenzenes, respectively, or the considerable magnitude of O_2 uncoupling by both enzymes. A hypothesis proposed for the uncoupled O_2 activation vs substrate monooxygenation by α-ketoglutarate dependent non-heme ferrous iron oxygenases,[47] an enzyme class that uses a different mechanism for O_2 activation than RDOs,[18,20−22] suggests that the lifetime of reactive Fe-oxygen species is one of the crucial factors. An extended lifetime of the Fe(IV)-oxo intermediate, for example, due to the presence of substrates reacting more slowly through electrophilic oxygen addition, could lead to uncoupled O_2 activation, as compared to more reactive substrates. No such trends are apparent in our data for 2NTBO and NBDO. Even though nitrotoluenes could be considered better substrates for electrophilic attack of Fe-oxygen species in 2NTDO and NBDO, they show $f_{O_2\text{-uc}}$ values identical to those of chlorinated and fluorinated nitrobenzenes. Instead, we hypothesize that the electronic properties of the substrate bound in the active site pocket exert some allosteric control of O_2 activation and could thus also be responsible for the efficiency of hydroxylation. We found recently for another RDO (naphthalene dioxygenase[35]) that the electron affinity of the substrate bound in the active site modulates the thermodynamics of the metal-to-substrate charge transfer from the Rieske cluster through the H_2O ligand in reaction **1** → **2** (Scheme 3). Given that the presence of the substrate is also accompanied by conformational changes in the active site that allow for O_2 binding at the non-heme Fe, we speculate that these processes result in an orientation of the substrate toward reactive Fe-oxygen species that is less likely to undergo O_2 uncoupling. Further theoretical studies on nitroarene dioxygenases are warranted to examine this hypothesis.

■ ENVIRONMENTAL SIGNIFICANCE

The observation of substantial O_2 uncoupling in almost all enzyme−substrate combinations investigated in our study suggests that the unproductive activation of O_2 is an important and largely overlooked path in the catalysis of contaminant oxygenation by nitroarene dioxygenases. Given that RDOs all share the catalytic mechanisms in which O_2 activation to reactive Fe-oxygen species occurs without interactions with the substrate,[18,20−22,35] we posit that O_2 uncoupling is likely an abundant phenomenon among RDOs. O_2 uncoupling is thus of relevance for many, if not most, contaminant dioxygenation pathways.[10,91] The relative extent of O_2 uncoupling observed among different substituted nitrobenzenes used as model substrates for the two nitroarene dioxygenases, however, is difficult to rationalize in terms of active site properties and simple structural and electronic descriptors of the substrates. Molecular structures of potential RDO substrates that would appear to favor dioxygenation may or may not be accompanied by O_2 uncoupling. The ambiguity of identifying productive enzyme−substrate combinations not only makes it very difficult to assess or even predict oxidative biodegradation in structure−reactivity relationships but also could challenge the interpretation of correlations of enzyme activity with productive contaminant transformation.[92]

The release of unreacted substrate during the O_2 uncoupling steps of the catalytic cycle of RDOs also has severe consequences for the assessment of the extent of contaminant transformation from changes of the isotopic composition in the remaining contaminant by compound-specific isotope analysis (CSIA).[93,94] Many applications of CSIA have demonstrated successfully that enzymatic catalysis of contaminant transformation can be tracked by the substrate isotope fractionation that arises from kinetic isotope effects of bond cleavage reactions. Unfortunately, the substrate-dependent occurrence of O_2 uncoupling modulates the extent of observable substrate isotope fractionation from isotope effects of aromatic compound hydroxylations by RDOs in an unpredictable way. This phenomenon likely precludes the quantitative interpretation of isotope fractionation associated with the dioxygenation processes. Our insights would therefore call for a re-evaluation of stable isotope based data from biodegradation reactions of various contaminants that are likely catalyzed through oxygenations by non-heme iron oxygenases[95−101] once the O_2 uncoupling behavior of the involved enzymes is known.

Finally, the quantitative evaluation of O_2 uncoupling reactions in enzyme assays presented in our study offers new avenues to study the hypothesis of ROS-driven adaptation of the RDO substrate spectrum toward new substances.[55−57] Besides having a potentially detrimental effect on RDO activity through enzyme self-hydroxylation[41] and redirecting metabolic fluxes to sustain defense mechanisms,[48] ROS generated from O_2 uncoupling have been postulated to increase mutation rate and selective pressure that lead to an accelerated adaptation of RDOs to xenobiotic compounds. In fact, 2NTDO and NBDO studied here originate from single isolated bacteria that might not necessarily represent the best or most common versions of the enzymes. Under laboratory conditions, shifts of substrate

https://doi.org/10.1021/acsenvironau.2c00023
ACS Environ. Au 2022, 2, 428−440

specificity of RDOs can occur within relatively short time scales of weeks to months[76,102] and they have been accompanied by mutations of selected amino acid residues unrelated to the enzymes' active site. Given that O_2 uncoupling and generation of ROS is potentially one of the first biochemical responses to exposure to new or alternate substrates, an evaluation of $f_{O_2\text{-uc}}$ values for RDOs with different degrees of adaptation to new substrates are needed. Such works would also allow further evaluation of the current substrate specificities of 2NTDO and NBDO as a possible evolutionary compromise to minimize oxidative stress triggered by the continuous exposure to mixtures of structurally similar contaminants in the environment.

■ ASSOCIATED CONTENT

Supporting Information

The Supporting Information is available free of charge at https://pubs.acs.org/doi/10.1021/acsenvironau.2c00023.

Chemicals and biological materials used, detailed method descriptions for protein purification, enzyme assays, chemical, and isotopic analyses, additional results on enzyme kinetics, reaction stoichiometries, and carbon and oxygen isotope fractionation (PDF)

■ AUTHOR INFORMATION

Corresponding Author

Thomas B. Hofstetter − *Eawag, Swiss Federal Institute of Aquatic Science and Technology, 8600 Dübendorf, Switzerland; Institute of Biogeochemistry and Pollutant Dynamics (IBP), ETH Zürich, 8092 Zürich, Switzerland;* orcid.org/0000-0003-1906-367X; Phone: +41 58 765 50 76; Email: thomas.hofstetter@eawag.ch; Fax: +41 58 765 50 28

Authors

Charlotte E. Bopp − *Eawag, Swiss Federal Institute of Aquatic Science and Technology, 8600 Dübendorf, Switzerland; Institute of Biogeochemistry and Pollutant Dynamics (IBP), ETH Zürich, 8092 Zürich, Switzerland*

Nora M. Bernet − *Eawag, Swiss Federal Institute of Aquatic Science and Technology, 8600 Dübendorf, Switzerland;* orcid.org/0000-0003-0200-0584

Hans-Peter E. Kohler − *Eawag, Swiss Federal Institute of Aquatic Science and Technology, 8600 Dübendorf, Switzerland;* orcid.org/0000-0001-7667-0762

Complete contact information is available at: https://pubs.acs.org/10.1021/acsenvironau.2c00023

Notes

The authors declare no competing financial interest.

■ ACKNOWLEDGMENTS

This work was supported by SNF grant 200021 172950-1. We thank Rebecca E. Parales for providing *E. coli* clones expressing NBDO and 2NTDO as well as Jakov Bolotin for analytical and experimental support.

■ REFERENCES

(1) Schwarzenbach, R. P.; Gschwend, P. M.; Imboden, D. M. *Environmental Organic Chemistry*, 3rd ed.; John Wiley & Sons, 2017; p 1005.

(2) Rojo, F., Ed. *Aerobic Utilization of Hydrocarbons, Oils, and Lipids*, 2nd ed.; Handbook of Hydrocarbon and Lypid Microbiology; Springer, 2019. DOI: 10.1007/978-3-319-50418-6.

(3) Fuchs, G.; Boll, M.; Heider, J. Microbial degradation of aromatic com498 pounds - from one strategy to four. *Nat. Rev. Microbiol.* **2011**, *9*, 803−816.

(4) Bugg, T. D. H. *Introduction to Enzyme and Coenzyme Chemistry*, 3rd ed.; Blackwell Publishing Ltd., 2012. DOI: 10.1002/9781118348970.

(5) Aukema, K. G.; Escalante, D. E.; Maltby, M. M.; Bera, A. K.; Aksan, A.; Wackett, L. P. *In silico* identification of bioremediation potential: Carbamazepine and other recalcitrant personal care products. *Environ. Sci. Technol.* **2017**, *51*, 880−888.

(6) Peng, R.; Xiong, A.; Xue, Y.; Fu, X.; Gao, F.; Zhao, W.; Tian, Y.; Yao, Q. Microbial biodegradation of polyaromatic hydrocarbons. *FEMS Microbiol Rev.* **2008**, *32*, 927−955.

(7) Jouanneau, Y.; Meyer, C.; Jakoncic, J.; Stojanoff, V.; Gaillard, J. Characterization of a naphthalene dioxygenase endowed with an exceptionally broad substrate specificity toward polycyclic aromatic hydrocarbons. *Biochemistry* **2006**, *45*, 12380−12391.

(8) Pieper, D.; Seeger, M. Bacterial metabolism of polychlorinated biphenyls. *J. Mol. Microbiol Biotechnol* **2008**, *15*, 121−138.

(9) Ju, K.-S.; Parales, R. E. Nitroaromatic compounds, from synthesis to biodegradation. *Microbiol. Mol. Biol. Rev.* **2010**, *74*, 250−272.

(10) Gibson, D. T.; Parales, R. E. Aromatic hydrocarbon dioxygenases in environmental biotechnology. *Curr. Opin. Biotechnol.* **2000**, *11*, 236−243.

(11) Bopp, C. E.; Kohler, H.-P. E.; Hofstetter, T. B. Enzyme kinetics of organic contaminant oxygenations. *Chimia* **2020**, *74*, 108−114.

(12) Chen, Q.; Wang, C. H.; Deng, S. K.; Wu, Y.-D.; Li, Y.; Yao, L.; Jiang, J. D.; Yan, X.; He, J.; Li, S. P. Novel three-component Rieske non-heme iron oxygenase system catalyzing the N-dealkylation of chloroacetanilide herbicides in sphingomonads DC-6 and DC-2. *Appl. Environ. Microbiol.* **2014**, *80*, 5078−5085.

(13) Dumitru, R.; Jiang, W. Z.; Weeks, D. P.; Wilson, M. A. Crystal structure of dicamba monooxygenase: A Rieske nonheme oxygenase that catalyzes oxidative demethylation. *J. Mol. Biol.* **2009**, *392*, 498−510.

(14) D'Ordine, R. L.; Rydel, T. J.; Storek, M. J.; Sturman, E. J.; Moshiri, F.; Bartlett, R. K.; Brown, G. R.; Eilers, R. J.; Dart, C.; Qi, Y.; Flasinski, S.; Franklin, S. J. Dicamba monooxygenase: Structural insights into a dynamic Rieske oxygenase that catalyzes an exocyclic monooxygenation. *J. Mol. Biol.* **2009**, *392*, 481−497.

(15) Barry, S. M.; Challis, G. L. Mechanism and catalytic diversity of Rieske non-heme iron-dependent oxygenases. *ACS Catal.* **2013**, *3*, 2362−2370.

(16) Münch, J.; Püllmann, P.; Zhang, W.; Weissenborn, M. J. Enzymatic hydroxylations of sp^3-carbons. *ACS Catal.* **2021**, *11*, 9168−9203.

(17) Solomon, E. I.; Brunold, T. C.; Davis, M. I.; Kemsley, J. N.; Lee, S. K.; Lehnert, N.; Neese, F.; Skulan, A. J.; Yang, Y. S.; Zhou, J. Geometric and electronic structure/function correlations in non-heme iron enzymes. *Chem. Rev.* **2000**, *100*, 235−349.

(18) Solomon, E. I.; Goudarzi, S.; Sutherlin, K. D. O_2 activation by non-heme iron enzymes. *Biochemistry* **2016**, *55*, 6363−6374.

(19) Solomon, E. I.; DeWeese, D. E.; Babicz, J. T. Mechanisms of O_2 activation by mononuclear non-heme iron enzymes. *Biochemistry* **2021**, *60*, 3497−3506.

(20) Costas, M.; Mehn, M.; Jensen, M.; Que, L. Dioxygen activation at mononuclear nonheme iron active sites: Enzymes, models, and intermediates. *Chem. Rev.* **2004**, *104*, 939−986.

(21) Kal, S.; Que, L. Dioxygen activation by nonheme iron enzymes with the 2-His-1-carboxylate facial triad that generate high-valent oxoiron oxidants. *J. Biol. Inorg. Chem.* **2017**, *22*, 339−365.

(22) Kovaleva, E. G.; Lipscomb, J. D. Versatility of biological non-heme Fe(II) centers in oxygen activation reactions. *Nat. Chem. Biol.* **2008**, *4*, 186−193.

(23) Bruijnincx, P. C. A.; van Koten, G.; Klein Gebbink, R. J. M. Mononuclear non-heme iron enzymes with the 2-His-1-carboxylate

facial triad: recent developments in enzymology and modeling studies. *Chem. Soc. Rev.* **2008**, *37*, 2716−2730.
(24) Ferraro, D. J.; Gakhar, L.; Ramaswamy, S. Rieske business: Structure-function of Rieske non-heme oxygenases. *Biochem. Biophys. Res. Commun.* **2005**, *338*, 175−190.
(25) Sydor, P. K.; Barry, S. M.; Odulate, O. M.; Barona-Gomez, F.; Haynes, S. W.; Corre, C.; Song, L.; Challis, G. L. Regio- and stereodivergent antibiotic oxidative carbocyclizations catalysed by Rieske oxygenase-like enzymes. *Nat. Chem.* **2011**, *3*, 388−392.
(26) Perry, C.; de Los Santos, E.; Alkhalaf, L.; Challis, G. Rieske non-heme iron-dependent oxygenases catalyse diverse reactions in natural product biosynthesis. *Nat. Prod. Rep.* **2018**, *35*, 622−632.
(27) Jiang, W.; Wilson, M. A.; Weeks, D. P. O-Demethylations catalyzed by Rieske nonheme iron monooxygenases involve the difficult oxidation of a saturated C−H Bond. *ACS Chem. Biol.* **2013**, *8*, 1687−1691.
(28) Schuster, J.; Schafer, F.; Hubler, N.; Brandt, A.; Rosell, M.; Hartig, C.; Harms, H.; Muller, R. H.; Rohwerder, T. Bacterial degradation of tert-amyl alcohol proceeds via hemiterpene 2-methyl-3-buten-2-ol by employing the tertiary alcohol desaturase function of the Rieske nonheme mononuclear iron oxygenase MdpJ. *J. Bacteriol.* **2012**, *194*, 972−981.
(29) Blomberg, M. R. A.; Borowski, T.; Himo, F.; Liao, R.-Z.; Siegbahn, P. E. M. Quantum chemical studies of mechanisms for metalloenzymes. *Chem. Rev.* **2014**, *114*, 3601−3658.
(30) Ohta, T.; Chakrabarty, S.; Lipscomb, J. D.; Solomon, E. I. Near-IR MCD of the non-heme ferrous active ste in naphthalene 1,2-dioxygenase: Correlation to crystallography and structural Insight into the mechanism of Rieske dioxygenases. *J. Am. Chem. Soc.* **2008**, *130*, 1601−1610.
(31) Sutherlin, K. D.; et al. NRVS Studies of the peroxide shunt intermediate in a Rieske dioxygenase and its relation to the native $Fe^{II}O_2$ reaction. *J. Am. Chem. Soc.* **2018**, *140*, 5544−5559.
(32) Rivard, B. S.; Rogers, M. S.; Marell, D. J.; Neibergall, M. B.; Chakrabarty, S.; Cramer, C. J.; Lipscomb, J. D. Rate-determining attack on substrate precedes Rieske cluster oxidation during *cis*-dihydroxylation by benzoate dioxygenase. *Biochemistry* **2015**, *54*, 4652−4664.
(33) Wolfe, M. D.; Parales, J. V.; Gibson, D. T.; Lipscomb, J. D. Single turnover chemistry and regulation of O_2 activation by the oxygenase component of naphthalene 1,2-dioxygenase. *J. Biol. Chem.* **2001**, *276*, 1945−1953.
(34) Wolfe, M. D.; Lipscomb, J. D. Hydrogen peroxide-coupled *cis*-diol formation catalyzed by naphthalene 1,2-dioxygenase. *J. Biol. Chem.* **2003**, *278*, 829−835.
(35) Csizi, K.-S.; Eckert, L.; Brunken, C.; Hofstetter, T. B.; Reiher, M. The apparently unreactive substrate facilitates the electron transfer for dioxygen activation in Rieske dioxygenases. *Chem.—Eur. J.* **2022**, *28*, e202103937.
(36) Sutherlin, K. D.; Liu, L. V.; Lee, Y.-M.; Kwak, Y.; Yoda, Y.; Saito, M.; Kurokuzu, M.; Kobayashi, Y.; Seto, M.; Que, L., Jr; Nam, W.; Solomon, E. I. Nuclear resonance vibrational spectroscopic definition of peroxy intermediates in nonheme iron sites. *J. Am. Chem. Soc.* **2016**, *138*, 14294−14302.
(37) Karlsson, A.; Parales, J. V.; Parales, R. E.; Gibson, D. T.; Eklund, H.; Ramaswamy, S. Crystal structure of naphthalene dioxygenase: Side-on binding of dioxygen to iron. *Science* **2003**, *299*, 1039−1042.
(38) Pabis, A.; Geronimo, I.; Paneth, P. A DFT study of the *cis*-dihydroxylation of nitroaromatic compounds catalyzed by nitrobenzene dioxygenase. *J. Phys. Chem. B* **2014**, *118*, 3245−3256.
(39) Bassan, A.; Blomberg, M. R. A.; Siegbahn, P. E. M. A theoretical study of the *cis*-dihydroxylation mechanism in naphthalene 1,2-dioxygenase. *J. Biol. Inorg. Chem.* **2004**, *9*, 439−452.
(40) Pati, S. G.; Kohler, H.-P. E.; Pabis, A.; Paneth, P.; Parales, R. E.; Hofstetter, T. B. Substrate and enzyme specificity of the kinetic isotope effects associated with the dioxygenation of nitroaromatic contaminants. *Environ. Sci. Technol.* **2016**, *50*, 6708−6716.
(41) Mantri, M.; Zhang, Z.; McDonough, M.; Schofield, C. Autocatalysed oxidative modifications to 2-oxoglutarate dependent oxygenases. *FEBS J.* **2012**, *279*, 1563−1575.
(42) Lee, K. Benzene-induced uncoupling of naphthalene dioxygenase activity and enzyme inactivation by production of hydrogen peroxide. *J. Bacteriol.* **1999**, *181*, 2719−2725.
(43) Thrower, J.; Mirica, L. M.; McCusker, K. P.; Klinman, J. P. Mechanistic Investigations of 1-Aminocyclopropane 1-Carboxylic Acid Oxidase with Alternate Cyclic and Acyclic Substrates. *Biochemistry* **2006**, *45*, 13108−13117.
(44) Dix, T. A.; Benkovic, S. J. Mechanism of "uncoupled" tetrahydropterin oxidation by phenylalanine hydroxylase. *Biochemistry* **1985**, *24*, 5839−5846.
(45) Iyer, S. R.; Chaplin, V. D.; Knapp, M. J.; Solomon, E. I. O_2 activation by nonheme Fe^{II} α-ketoglutarate-dependent enzyme variants: Elucidating the role of the facial triad carboxylate in FIH. *J. Am. Chem. Soc.* **2018**, *140*, 11777−11783.
(46) Bünz, P. V.; Cook, A. M. Dibenzofuran 4, 4a-dioxygenase from Sphingomonas sp. strain RW1: angular dioxygenation by a three-component enzyme system. *J. Bacteriol.* **1993**, *175*, 6467−6475.
(47) McCusker, K. P.; Klinman, J. P. Modular behavior of tauD provides insight into the origin of specificity in α-ketoglutarate-dependent nonheme iron oxygenases. *Proc. Natl. Acad. Sci. U. S. A.* **2009**, *106*, 19791−19795.
(48) Nikel, P. I.; Fuhrer, T.; Chavarría, M.; Sánchez-Pascuala, A.; Sauer, U.; de Lorenzo, V. Reconfiguration of metabolic fluxes in Pseudomonas putida as a response to sub-lethal oxidative stress. *ISME J.* **2021**, *15*, 1751−1766.
(49) Ponce, B.; Latorre, V.; González, M.; Seeger, M. Antioxidant compounds improved PCB-degradation by Burkholderia strain LB400. *Enzyme Microb Technol.* **2011**, *49*, 509−516.
(50) Bertini, I.; Gray, H. B.; Stiefel, E. I.; Selverstone Valentine, J. *Biological Inorganic Chemistry: Structure and Reactivity*; University Science Books, 2007.
(51) Selverstone Valentine, J., Foote, C. S., Greenberg, A., Liebman, J. F., Eds. *Active Oxygen in Biochemistry*; Springer Netherlands: Dordrecht, 1995; Vol. 3; p 463. DOI: 10.1007/978-94-011-0609-2.
(52) Patrauchan, M. A.; Florizone, C.; Eapen, S.; Gomez-Gil, L.; Sethuraman, B.; Fukuda, M.; Davies, J.; Mohn, W. W.; Eltis, L. D. Roles of ring-hydroxylating dioxygenases in styrene and benzene catabolism in *Rhodococcus jostii* RHA1. *J. Bacteriol.* **2008**, *190*, 37−47.
(53) Chávez, F.; Lünsdorf, H.; Jerez, C. Growth of polychlorinated-biphenyl-degrading bacteria in the presence of biphenyl and chlorobiphenyls generates oxidative stress and massive accumulation of inorganic polyphosphate. *Appl. Environ. Microbiol.* **2004**, *70*, 3064−3072.
(54) Agulló, L.; Cámara, B.; Martínez, P.; Latorre, V.; Seeger, M. Response to 668 (chloro)biphenyls of the polychlorobiphenyl-degrader *Burkholderia xenovorans* LB400 involves stress proteins also induced by heat shock and oxidative stress. *FEMS Microbiol Lett.* **2007**, *267*, 167−175.
(55) Pérez-Pantoja, D.; Nikel, P. I.; Chavarría, M.; de Lorenzo, V. Transcriptional control of 2,4-dinitrotoluene degradation in Burkholderia sp. R34 bears a regulatory patch that eases pathway evolution. *Environ. Microbiol.* **2021**, *23*, 2522−2531.
(56) Pérez-Pantoja, D.; Nikel, P. I.; Chavarria, M.; de Lorenzo, V. Endogenous stress caused by faulty oxidation reactions fosters evolution of 2,4-dinitrotoluene-degrading bacteria. *PLoS Genet.* **2013**, *9*, e1003764.
(57) Ilmjärv, T.; Naanuri, E.; Kivisaar, M. Contribution of increased mutagenesis to the evolution of pollutants-degrading indigenous bacteria. *PLoS One* **2017**, *12*, e0182484.
(58) Lessner, D. J.; Johnson, G. R.; Parales, R. E.; Spain, J. C.; Gibson, D. T. Molecular characterization and substrate specificity of nitrobenzene dioxygenase from Comamonas sp strain JS765. *Appl. Environ. Microbiol.* **2002**, *68*, 634−641.
(59) Parales, J. V.; Parales, R. E.; Resnick, S. M.; Gibson, D. T. Enzyme specificity of 2-nitrotoluene 2,3-dioxygenase from Pseudomonas sp. strain JS42 is determined by the C-terminal region of the alpha subunit of the oxygenase component. *J. Bacteriol.* **1998**, *180*, 1194−1199.
(60) Pati, S. G.; Kohler, H.-P. E.; Bolotin, J.; Parales, R. E.; Hofstetter, T. B. Isotope Effects of Enzymatic Dioxygenation of Nitrobenzene and

2-Nitrotoluene by Nitrobenzene Dioxygenase. *Environ. Sci. Technol.* **2014**, *48*, 10750−10759.
(61) Pati, S. G.; Kohler, H.-P. E.; Hofstetter, T. B. In *Measurement and Analysis of Kinetic Isotope Effects*; Harris, M. E., Anderson, V. E., Eds.; Academic Press, 2017; pp 292−329. DOI: 10.1016/bs.mie.2017.06.044.
(62) Pabis, A.; Geronimo, I.; York, D. M.; Paneth, P. Molecular dynamics simulation of nitrobenzene dioxygenase using AMBER force field. *J. Chem. Theory Comput.* **2014**, *10*, 2246−2254.
(63) Geronimo, I.; Paneth, P. A DFT and ONIOM study of C-H hydroxylation catalyzed by nitrobenzene 1,2-dioxygenase. *Phys. Chem. Chem. Phys.* **2014**, *16*, 13889−13899.
(64) Friemann, R.; Ivkovic-Jensen, M. M.; Lessner, D. J.; Yu, C. L.; Gibson, D. T.; Parales, R. E.; Eklund, H.; Ramaswamy, S. Structural insight into the dioxygenation of nitroarene compounds: the crystal structure of nitrobenzene dioxygenase. *J. Mol. Biol.* **2005**, *348*, 1139−1151.
(65) Pati, S. G.; Bopp, C. E.; Kohler, H.-P. E.; Hofstetter, T. B. Substrate-specific coupling of O_2 activation to hydroxylation of aromatic compounds by Rieske non-heme iron dioxygenases. *ACS Catal.* **2022**, *12*, 6444−6456.
(66) Lee, K. S.; Parales, J. V.; Friemann, R.; Parales, R. E. Active site residues controlling substrate specificity in 2-nitrotoluene dioxygenase from Acidovorax sp strain JS42. *J. Ind. Microbiol. Biotechnol.* **2005**, *32*, 465−473.
(67) Zhu, H.; Peck, S. C.; Bonnot, F.; van der Donk, W. A.; Klinman, J. P. Oxygen-18 kinetic isotope effects of nonheme iron ezymes HEPD and MPnS support ron(III) superoxide as the hydrogen abstraction species. *J. Am. Chem. Soc.* **2015**, *137*, 10448−10451.
(68) Mirica, L. M.; McCusker, K. P.; Munos, J. W.; Liu, H.-w.; Klinman, J. P. ^{18}O Kinetic isotope effects in non-heme iron enzymes: Probing the nature of Fe/O_2 intermediates. *J. Am. Chem. Soc.* **2008**, *130*, 8122−8123.
(69) Tian, G.; Klinman, J. Discrimination between ^{16}O and ^{18}O in oxygen-binding to the reversible oxygen carriers hemoglobin, myoglobin, hemerythrin, and hemocyanin - a new probe for oxygen-binding and reductive activation by proteins. *J. Am. Chem. Soc.* **1993**, *115*, 8891−8897.
(70) Roth, J. P.; Klinman, J. P. In *Isotope Effects in Chemistry and Biology*; Kohen, A., Limbach, H.-H., Eds.; CRC Press/Taylor & Francis: New York, 2006; pp 645−669. DOI: 10.1201/9781420028027.ch24.
(71) Roth, J. P. Oxygen isotope effects as probes of electron transfer mechanisms and structures of activated O_2. *Acc. Chem. Res.* **2009**, *42*, 399−408.
(72) Roth, J. P. Advances in studying bioinorganic reactions mechanisms: isotopic probes of activated oxygen intermediates in metalloenzymes. *Curr. Opin. Chem. Biol.* **2007**, *11*, 142−150.
(73) Lanci, M.; Roth, J. Oxygen isotope effects upon reversible O_2-binding reactions: Characterizing mononuclear superoxide and peroxide structures. *J. Am. Chem. Soc.* **2006**, *128*, 16006−16007.
(74) Wijker, R. S.; Pati, S. G.; Zeyer, J.; Hofstetter, T. B. Enzyme kinetics of different types of flavin-dependent monooxygenases determine the observable contaminant stable isotope fractionation. *Environ. Sci. Technol. Lett.* **2015**, *2*, 329−334.
(75) Parales, R. E.; Huang, R.; Yu, C. L.; Parales, J. V.; Lee, F. K. N.; Lessner, D. J.; Ivkovic-Jensen, M. M.; Liu, W.; Friemann, R.; Ramaswamy, S.; Gibson, D. T. Purification, characterization, and crystallization of the components of the nitrobenzene and 2-nitrotoluene dioxygease enzyme systems. *Appl. Environ. Microbiol.* **2005**, *71*, 3806−3814.
(76) Mahan, K.; Penrod, J.; Ju, K.; Al Kass, N.; Tan, W.; Truong, R.; Parales, J.; Parales, R. Selection for growth on 3-nitrotoluene by 2-nitrotoluene-utilizing Acidovorax sp. strain JS42 identifies nitroarene dioxygenases with altered specificities. *Appl. Environ. Microbiol.* **2015**, *81*, 309−319.
(77) Pati, S. G.; Bolotin, J.; Brennwald, M. S.; Kohler, H.-P. E.; Werner, R. A.; Hofstetter, T. B. Measurement of oxygen isotope ratios ($^{18}O/^{16}O$) of aqueous O_2 in small samples by gas chromatography/isotope ratio mass spectrometry. *Rapid Commun. Mass Spectrom.* **2016**, *30*, 684−690.
(78) Bopp, C. E.; Bolotin, J.; Pati, S. G.; Hofstetter, T. B. Managing argon interference in the measurement of oxygen isotope ratios ($^{18}O/^{16}O$) by continuous flow isotope ratio mass spectrometry. *Anal. Bioanal. Chem.* **2022**, in press.
(79) Bergmeyer, H. New values for the molar extinction coefficients of NADH and NADPH for the use in routine laboratories (authoras transl). *Z. Klin. Chem. Klin. Biochem.* **1975**, *13*, 507−508.
(80) Morlock, L.; Böttcher, D.; Bornscheuer, U. Simultaneous detection of NADPH consumption and H_2O_2 production using the Ampliflu^{TM}Red assay for screening of P450 activities and uncoupling. *Appl. Microbiol. Biotechnol.* **2018**, *102*, 985−994.
(81) Zhou, M.; Diwu, Z.; Panchuk-Voloshina, N.; Haugland, R. A stable nonfluorescent derivative of resorufin for the fluorometric determination of trace hydrogen peroxide: applications in detecting the activity of phagocyte NADPH oxidase and other oxidases. *Anal. Biochem.* **1997**, *253*, 162−168.
(82) An, D.; Gibson, D. T.; Spain, J. C. Oxidative release of nitrite from 2-nitrotoluene by a three-component enzyme system from *Pseudomonas* sp. strain JS42. *J. Bacteriol.* **1994**, *176*, 7462−7467.
(83) Barkan, E.; Luz, B. High-precision measurements of17O/16O and18O/16O of O2 and O2/Ar ratio in air. *Rapid Commun. Mass Spectrom.* **2003**, *17*, 2809−2814.
(84) Werner, R. A.; Brand, W. A. Referencing strategies and techniques in stable isotope ratio analysis. *Rapid Commun. Mass Spectrom.* **2001**, *15*, 501−519.
(85) Wijker, R. S.; Bolotin, J.; Nishino, S. F.; Spain, J. C.; Hofstetter, T. B. Using compound-specific isotope analysis to assess biodegradation of nitroaromatic explosives in the subsurface. *Environ. Sci. Technol.* **2013**, *47*, 6872−6883.
(86) Hofstetter, T. B.; Spain, J. C.; Nishino, S. F.; Bolotin, J.; Schwarzenbach, R. P. Identifying competing aerobic nitrobenzene biodegradation pathways using compound-specific isotope analysis. *Environ. Sci. Technol.* **2008**, *42*, 4764−4770.
(87) Gao, Y.; Palatucci, M. L.; Waidner, L. A.; Li, T.; Guo, Y.; Spain, J. C.; Zhou, N. A Nag-like dioxygenase initiates 3,4-dichloronitrobenzene degradation via 4,5-dichlorocatechol in Diaphorobacter sp. strain JS3050. *Environmental Microbiology* **2021**, *23*, 1053−1065.
(88) Palatucci, M. L.; Waidner, L. A.; Mack, E. E.; Spain, J. C. Aerobic biodegradation of 2,3- and 3,4-dichloronitrobenzene. *J. Hazard. Mater.* **2019**, *378*, 120717.
(89) Spain, J. C.; Hughes, J. B.; Knackmuss, H.-J. *Biodegradation of Nitroaromatic Compounds and Explosives*; Lewis Publishers: Boca Raton, FL, 2000; p 434. DOI: 10.1201/9781420032673.
(90) Mirica, L. M.; Klinman, J. P. The nature of O_2 activation by the ethylene-forming enzyme 1-aminocyclopropane-1-carboxylic acid oxidase. *Proc. Natl. Acad. Sci. U. S. A.* **2008**, *105*, 1814−1819.
(91) Wackett, L. P. Mechanism and applications of Rieske non-heme iron dioxygenases. *Enzyme Microb. Technol.* **2002**, *31*, 577−587.
(92) Fenner, K.; Elsner, M.; Lueders, T.; McLachlan, M. S.; Wackett, L. P.; Zimmermann, M.; Drewes, J. E. Methodological advances to study contaminant biotransformation: New prospects for understanding and reducing environmental persistence. *ACS ES&T Water* **2021**, *1*, 1541−1554.
(93) Hofstetter, T. B.; Schwarzenbach, R. P.; Bernasconi, S. M. Assessing transformation processes of organic compounds using stable isotope fractionation. *Environ. Sci. Technol.* **2008**, *42*, 7737−7743.
(94) Elsner, M.; Jochmann, M. A.; Hofstetter, T. B.; Hunkeler, D.; Bernstein, A.; Schmidt, T. C.; Schimmelmann, A. Current challenges in compound-specific stable isotope analysis of environmental organic contaminants. *Anal. Bioanal. Chem.* **2012**, *403*, 2471−2491.
(95) Pati, S. G.; Shin, K. A.; Skarpeli-Liati, M.; Bolotin, J.; Eustis, S. N.; Spain, J. C.; Hofstetter, T. B. Carbon and nitrogen isotope effects associated with the dioxygenation of aniline and diphenylamine. *Environ. Sci. Technol.* **2012**, *46*, 11844−11853.
(96) Liang, X.; Howlett, M. R.; Nelson, J. L.; Grant, G.; Dworatzek, S.; Lacrampe-Couloume, G.; Zinder, S. H.; Edwards, E. A.; Sherwood Lollar, B. Pathway-dependent isotope fractionation during aerobic and

anaerobic degradation of monochlorobenzene and 1,2,4-trichlorobenzene. *Environ. Sci. Technol.* **2011**, *45*, 8321−8327.
(97) Mancini, S. A.; Hirschorn, S. K.; Elsner, M.; Lacrampe-Couloume, G.; Sleep, B. E.; Edwards, E. A.; Sherwood Lollar, B. Effects of trace element concentration on enzyme controlled stable isotope fractionation during aerobic biodegradation of toluene. *Environ. Sci. Technol.* **2006**, *40*, 7675−7681.
(98) Musat, F.; Vogt, C.; Richnow, H.-H. Carbon and hydrogen stable isotope fractionation associated with the aerobic and anaerobic degradation of saturated and alkylated aromatic hydrocarbons. *J. Mol. Microbiol. Biotechnol.* **2016**, *26*, 211−226.
(99) Rakoczy, J.; Remy, B.; Vogt, C.; Richnow, H. H. A bench-scale constructed wetland as a model to characterize benzene biodegradation processes in freshwater wetlands. *Environ. Sci. Technol.* **2011**, *45*, 10036−10044.
(100) Feisthauer, S.; Vogt, C.; Modrzynski, J.; Szlenkier, M.; Kruger, M.; Siegert, M.; Richnow, H.-H. Different types of methane monooxygenases produce similar carbon and hydrogen isotope fractionation patterns during methane oxidation. *Geochim. Cosmochim. Acta* **2011**, *75*, 1173−1184.
(101) Vogt, G.; Cyrus, E.; Herklotz, I.; Schlosser, D.; Bahr, A.; Herrmann, S.; Richnow, H.-H.; Fischer, A. Evaluation of toluene degradation pathways by two-dimensional stable isotope fractionation. *Environ. Sci. Technol.* **2008**, *42*, 7793−7800.
(102) Ju, K. S.; Parales, R. E. Evolution of a new bacterial pathway for 4-nitrotoluene degradation. *Mol. Microbiol.* **2011**, *82*, 355−364.

https://doi.org/10.1021/acsenvironau.2c00023
ACS Environ. Au 2022, 2, 428−440